Application of synchrotron source based DEI method in guinea pig cochleae imaging*

YIN Hongxia[1], LIU Bo[2], GAO Xin[1], GAO Xiulai[2] and LUO Shuqian[1]**

(1. College of Biomedical Engineering, Capital University of Medical Sciences, Beijing 100069, China; 2. Department of Anatomy, Capital University of Medical Sciences, Beijing 100069, China)

Accepted on April 12, 2006

Abstract Hard X-ray diffraction enhanced imaging (DEI), which is based on a synchrotron source and monochromator-analyzer-crystal system, is an effective method for imaging X-ray phase shift. Utilizing an analyzer crystal with high angular sensitivity of micro-radian, DEI can measure the transmitted, refracted and scattered X-rays when projecting onto a sample. It dramatically improves the contrast and spatial resolution of the resultant images. At the topography station of Beijing Synchrotron Radiation Facilities (BSRF), we implemented DEI method in guinea pig cochleae imaging and acquired a series of DEI images. Based on these images, the apparent absorption and refraction images were calculated. The DEI images revealed the holistic spiral structures and inner details of guinea pig cochleae clearly, even including the structures at the cellular level, such as the static cilia of hairy cells and the limbus of Hansen cell. Due to the advantages of high contrast, high spatial resolution and distinct edge-enhanced effect, DEI method promises extensive applications in biology, medicine and clinic in the near future.

Keywords: diffraction enhanced imaging, hard X-ray imaging, phase-contrast imaging, cochlea, micro-structure, synchrotron source.

Hard X-ray phase-contrast imaging (PCI) is a new imaging technique that images the gradient distribution of X-ray phase shifts due to refraction caused by the object to be imaged[1—5]. Compared with the conventional absorption-based X-ray imaging techniques, PCI can increase the spatial resolution of the image about 1000 times[3,4]. PCI technique began in the middle of the 1990s[3—5], soon after became a hot issue in the world, and was studied in various application domains such as biological and medical researches, material science and non-destructive detecting, etc. Because of the high sensitivity of X-ray phase shifts to light element materials, PCI has become an effective way to observe the micro-structures of biological soft tissues[4,5].

To date, several hard X-ray phase-contract imaging methods have been developed to detect X-ray phase shifts. They fall into the following three general categories[6]: (1) interferometery[3,4,7,8]; (2) diffraction enhanced imaging (DEI)[5,9—14]; (3) in-line holography or Fresnel diffraction[15,16]. Among them, DEI, based on a synchrotron source and monochromator-analyzer-crystal system, utilizes an analyzer crystal with high angular sensitivity to measure the X-ray attenuation of the object, refraction, and small angle scattering, which dramatically improves the contrast and spatial resolution of the images[9]. In recent years, there are a lot of theoretical researches and applied researches about DEI, the former includes phase information separation and the latter includes breast cancer diagnosis, cartilage imaging, etc.[12—14,19,20]. This paper presents the application of DEI method to guinea pig cochleae imaging.

The cochleae are complex but vital micro-organs to generate hearing. The cochlear morphologic research is the basis of hearing research. Conventionally, the cochlear morphologic research relies on histological sections and whole mount stretch preparation which are observed under an optical or electron microscope[17,18]. In our study, DEI method was applied to the guinea pig cochleae imaging. The acquired DEI images successfully display the holistic spiral structures and inner details of the guinea pig cochleae without breaking its integrity. Compared with the conventional absorption-based image of the cochlea, DEI method achieved better contrast. Moreover, a series of DEI images corresponding to different angular points on the rocking curve of the analyzer crystal

* Supported by National Natural Science Foundation of China (Grant No. 60532090) and Beijing Natural Science Foundation (No. 7031001)

** To whom corresponce should be addressed. E-mail: sqluo@ieee.org

were obtained. Signal noise ratio (SNR) and figure of merit (FOM) were used to evaluate the serial DEI images and the imaging efficiency.

1 Principle of DEI

DEI setup is composed of a synchrotron source, a monochromator crystal, a sample desk, an analyzer crystal and a detector (Fig.1)[11]. The monochromator crystal is used to select the energy range of X-rays from the incident synchrotron beam and to generate a nearly monochromatic X-ray beam[9,10]. The monochromatic beam transmits through the sample to be imaged, then casts onto the analyzer crystal. After X-ray beam is diffracted and reflected by the analyzer crystal onto the detector, the DEI images are formed[9,10]. In the meridian plane, the analyzer crystal can be rotated within an angle range away from the monochromator crystal. While without a sample, fixing the monochromator crystal and rotating the analyzer crystal, the reflectivity of the analyzer crystal surface to the incident beam will vary along with different rotating angles. The function curve of reflectivity varying along with rotating angles is referred to as the natural rocking curve of the analyzer crystal[9]. The measured rocking curve in the experiment is given in Fig.2. According to Bragg's diffraction law, only X-rays satisfying Bragg condition of the analyzer crystal will be diffracted onto the detector[9]. In the energy range of hard X-ray, the full width half maximum (FWHM) of the analyzer rocking curve is about a few micro-radians, so the analyzer crystal has a high angular sensitivity[9,11].

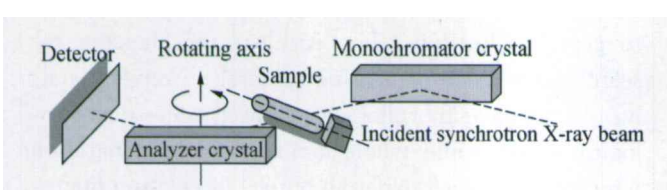

Fig. 1. DEI setup.

While X-ray beam transmits through a sample, the interactions between X-ray and the sample mainly involve X-ray absorption, refraction, scattering and diffraction. All of them contribute to the resultant images[9,11]. Due to the small angle range of X-ray refraction, scattering and diffraction, in the conventional X-ray imaging methods, information from X-ray refraction, scattering and diffraction inside the sample are not detectable. But DEI successfully separates all of them utilizing an analyzer crystal with high angular sensitivity. Because of the analyzer crystal with an acceptance angle range of only a few micro-radians, DEI automatically provides scattering and diffraction rejection of X-ray in a high degree, which is named as extinction contrast[9]. Therefore, DEI images mainly contain contrasts from X-ray absorption, refraction, extinction and small-angle scattering (scattering angles less than milliradian)[9,10,12]. If the small-angle scattering could be ignored, DEI could separate the refraction information from others and then the apparent absorption and refraction images would be obtained[9]. The contrast of the apparent refraction image mainly comes from the refraction index gradient distribution of X-ray inside the object while the contrast of the apparent absorption image comes from the combination of absorption and extinction[9]. Since the maximum refraction index gradient lies on the edge of different tissues inside the object, it is shown as distinct edge-enhanced effect in the refraction-based images.

When the analyzer crystal is turned away from the Bragg angle and locates at the symmetric points of $\theta=\theta_L$(L means low angle side) and $\theta=\theta_H$(H means high angle side) on the two shoulders of the rocking curve respectively, two images can be obtained: the low angle image I_L and the high angle image I_H(I_L and I_H all hold apparent absorption contrast and refraction index gradient information)[9,10]. We denote θ_L as the relative angle of the incident X-ray away from the Bragg angle, $R(\theta)$ as the reflectivity of the analyzer crystal, then the fundamental equations (1a) and (1b) can be obtained[9,10]:

$$I_M=\frac{I_L\left(\frac{dR}{d\theta}\right)(\theta_H)-I_H\left(\frac{dR}{d\theta}\right)(\theta_L)}{R(\theta_L)\left(\frac{dR}{d\theta}\right)(\theta_H)-R(\theta_H)\left(\frac{dR}{d\theta}\right)(\theta_L)}, \tag{1a}$$

$$\Delta\theta_Z=\frac{I_HR(\theta_L)-I_LR(\theta_H)}{I_L\left(\frac{dR}{d\theta}\right)(\theta_H)-I_H\left(\frac{dR}{d\theta}\right)(\theta_L)}. \tag{1b}$$

In the equations, I_M is the modified intensity of X-ray in the acceptance angle range of the analyzer crystal after X-ray transmitting the sample and $\Delta\theta_Z$ is the angle deviation of X-ray in the vertical plane respect to diffraction plane of the analyzer crystal. The apparent absorption and refraction images can be obtained by the pixel-to-pixel computing with the images I_L and I_H according to Eqs. (1a) and (1b)[13].

$[(dR/d\theta)(\theta_L)]$ and $[(dR/d\theta)(\theta_H)]$ are the slopes at the points of θ_L and θ_H on the rocking curve

respectively, while $R(\theta_L)$ and $R(\theta_H)$ are the reflectivity at these two points respectively. In order to simplify the equations, we denote $s_L = [(dR/d\theta)(\theta_L)]$, $s_H = [(dR/d\theta)(\theta_H)]$, $r_L = R(\theta_L)$ and $r_H = R(\theta_H)$. s_L, s_H, r_L and r_H are all constants at certain points of θ_L and θ_H. Substituting them into Eqs. (1a) and (1b), Eqs. (2a) and (2b) can be deduced:

$$I_M = \frac{I_L s_H - I_H s_L}{r_L s_H - r_H s_L}, \tag{2a}$$

$$\Delta\theta_Z = \frac{I_H r_L - I_L r_H}{I_L s_H - I_H s_L}. \tag{2b}$$

Under the ideal condition, the equations of $\theta_L = -\theta_H$, $s_L = -s_H = S(S>0)$, $r_L = r_H = R(R>0)$ are tenable at the symmetric points of θ_L and θ_H on the rocking curve. Then Eqs. (2a) and (2b) can be simplified into Eqs. (3a) and (3b) respectively[10]:

$$I_M = \frac{1}{2R}(I_L + I_H), \tag{3a}$$

$$\Delta\theta_Z = -\frac{R}{S}\frac{I_H - I_L}{I_H + I_L}. \tag{3b}$$

From Eqs. (3a) and (3b), it can be seen that computing the apparent absorption and refraction images can be simplified into adding and subtracting the low and high angle images. However, it is very difficult to select the exactly symmetric points of θ_L and θ_H in experiments. When the selected points on the rocking curve have very small deviations from the ideal points, the apparent absorption and refraction images can be computed out using Eqs. (2a) and (2b) by weighting DEI images acquired at the approximatively symmetric points on the rocking curve.

2 The experiments

2.1 The setup

The experiments were performed using beamline 4W1A at the topography station of Beijing Synchrotron Radiation Facilities (BSRF). The double-crystal DEI setup (Fig.1), which was constructed at the topography station of BSRF[11], was used in the experiments. Two crystals of the same type of silicon (111) were used as monochromator and analyzer. A series of DEI images, including the low and high angle images and peak image, were obtained with tuning the analyzer crystal respect to different points on the rocking curve.

Two types of detectors were used in our experiments: X-ray fast digital imager (FDI) camera system with a spatial resolution of 10.9 μm and Fuji IX80 X-ray film with a resolution of 0.3—0.8 μm. The images recorded by FDI camera were directly stored in the computer and synchronously shown on the screen, while ones recorded by the X-ray films needed to be developed, fixed, observed under the light microscope, then digitalized and input into the computer.

The conventional radiography experimental setup based on the synchrotron source was formed by changing DEI setup: setting the monochromator and analyzer crystals parallel, placing the sample behind two crystals and close to the detector. With this modified setup, the conventional absorption-based images were obtained and taken for comparison with DEI images. In this setup, two crystals were used as double-crystal monochromator so that the energy of the monochromatic X-ray decreased a little.

2.2 The X-ray source

The synchrotron beam source is 0.3 μrad of maximum horizontal angle and 0.5 μrad of maximum vertical angle. The incident beam from beamline 4W1A is nearly parallel at the entrance to the experimental hutch, which is 43 m far from the beam source. The range of stream intensity is 50—100 mA and the intensity attenuates exponentially. The tunable energy range of the X-ray beam is 3—22 keV. The aperture of the beam used for the experiments was 20 mm high and 8 mm wide. In our experiments, the monochromatic beam energies of 8 keV, 9.4 keV, 10 keV and higher energy of 16 keV were used in imaging the guinea pig cochleae and various measurements were acquired.

2.3 Subjects and treatments

The guinea pig cochleae were selected as the subjects. In the earlier experiments, twelve guinea pig cochleae underwent different treatments were divided into six groups and there were two subjects in each group, which is clearly shown in Table 1. The treatments of the cochleae included decalcification, staining with silver nitrate solution, and reduction (see below). The subjects of the first group did not undergo any treatments and those in other groups underwent different combined treatments. The experimental results showed that decalcification of the cochlea improved the contrast and quality of the resultant im-

ages obviously, while staining and reduction had less help for improving image quality. Therefore, the decalcified cochleae of guinea pigs were selected in the latter experiments.

Table 1. Subjects grouped by different treatments

Groups	Decalcification	Staining	Reduction
1			
2	+		
3	+	+	
4	+	+	+
5		+	
6		+	+

Annotation: " + " means that the subjects underwent the corresponding treatment.

In the earlier experiments, the subjects were prepared in accordance with the following procedure:

(1) Twelve guinea pigs were sacrificed by perfusing with 0.9% sodium solution and 4% polyformaldehyde solution. Both sides of the cochleae were carefully taken out, then, removing the footplates of stapes, puncturing through the membranes of round window, and immersing the cochleae into 30% saccharose formaldehyde solution for 24 hours.

(2) The cochleae were taken out from fixation solution and washed with distilled water for 6 hours. Then, 3 to 5 days' decalcification with Plank's solution was accomplished, which was the key step.

(3) Staining by immersing the cochleae into 1.5% silver nitrate solution for 7 days at 37℃ in dark. The silver nitrate solution was replaced every other day.

(4) The cochleae were immersed into intopyrogallol acid solution for one day for reduction after being washed with distilled water.

(5) All treated cochleae were fully washed with 0.1 mol/L phosphate buffer solution (PBS) and then preserved in 4% polyformaldehyde solution.

In the subsequent experiments, the cochleae underwent only fixation and decalcification without staining or reduction.

2.4 Methods

At first, the natural rocking curve of the analyzer crystal was scanned without the sample. Fig.2 illustrates the measured analyzer rocking curve in the energy of 9.4 keV of the monochromatic X-ray. The interval of the sample points on the curve is 0.2″ (0.2″ = 0.97 μrad). The full width half maximum ($W_D/2$) of the measured rocking curve is about 10″ (48.5 μrad). Then, the cochleae were fixed on the sample desk after being cut off the unnecessary tissues carefully and exposed at 23℃ for 10 min.

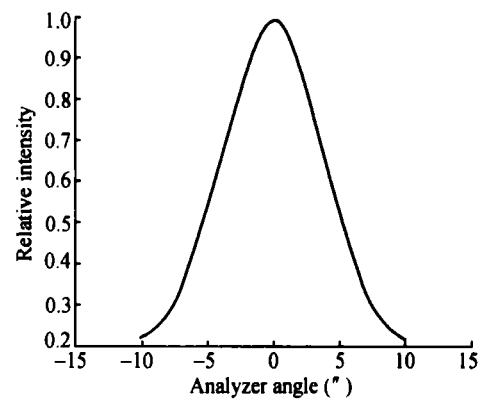

Fig. 2. The measured rocking curve of the analyzer crystal in the experiment. The energy of X-ray was 9.4 keV and stream intensity was 54 mA.

A series of points were selected on the rocking curve at an equal interval of 1″ (4.85 μrad) (Fig.3). A series of DEI images of the cochleae were acquired with the analyzer tuned to the corresponding points of the rocking curve. The measurements were recorded by X-ray films or FDI camera.

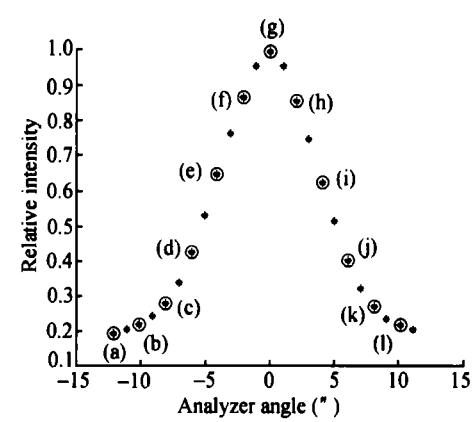

Fig. 3. The selected points on the rocking curve in DEI imaging. The energy of X-ray was 9.4 keV and stream intensity was 54 mA.

For comparing with DEI images, the conventional absorption-based images of the cochleae were taken using the modified setup by setting two crystals parallel as double-crystal monochromator, fixing the sample behind the crystals and close to the detector.

3 Results and discussion

In the earlier experiments, the acquired DEI images of the guinea pig cochleae which underwent different treatments (shown in Table 1) including decalcification, staining with silver nitrate solution, and reduction showed that the DEI images of the decalcified cochleae displayed the cochlear inner details clearly, but those without cochleae decalcification were burry because of the difficulty of being transmitted through. Even the energy of X-ray being increased to 16 keV, the images of the cochleae without decalcification were not obviously improved. All these demonstrated that decalcification can greatly improve the image quality, while staining with silver nitrate solution or reduction has no obvious help. As it is analyzed, the main reason is that decalcification reduces the density of cochleae to be close to the density of soft tissues so that X-ray can easily transmit through the cochleae and the resultant image quality is improved. In addition, DEI also contributes to image quality improvement, because DEI technique is highly sensitive to soft tissues. Therefore, we selected guinea pig cochleae which underwent decalcification as subjects in the latter experiments.

3.1 DEI images recorded by X-ray films

Fig.4 (a) shows one peak image of the decalcified cochlea and Fig.4 (b) gives its magnified image of the selected region. The detector was X-ray film. Fig.4 (a) displays clearly the spiral structure and inner details of the cochlea and has got a high contrast and good spatial resolution. The partially magnified image shown in Fig.4 (b) displays more details. According to anatomy of the inner ear and the atlas of inner ear, we labeled the microstructures in the image (Fig. 4). In Fig. 4 (a), besides the macroscopic structures of bone labyrinth, membranous labyrinth, modiolus (label 8), spiral lamina (label 4), spiral prominence of the spiral ligament (label 9), etc., more microcosmic structures even at cellular level are identified clearly, such as basilar membrane, vestibular membrane, basilar membranous crest, static cilia of hairy cells and limbus of Hansen cell. It is demonstrated that DEI technique is an effective method to observe cochlea and other biological micro-organs and has the potential to imaging at cellular-level. It is possible that DEI becomes a better morphologic research method than the optic and electron microscopies because DEI can preserve the integrated structure of the biological tissue, and at the same time, achieving a very high contrast and good spatial resolution.

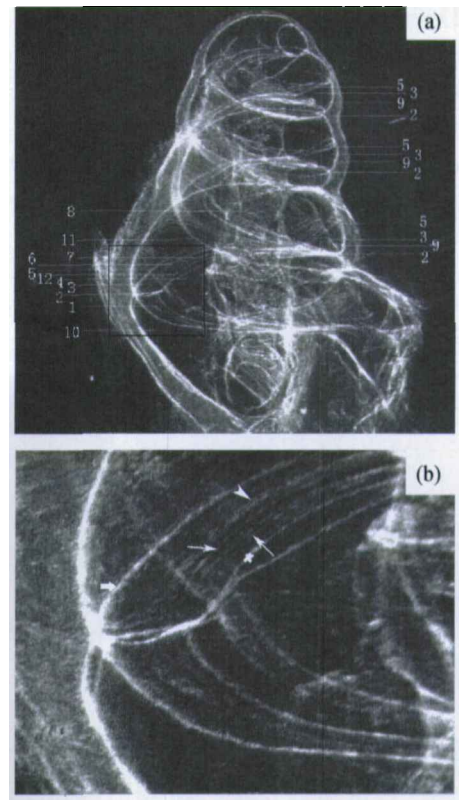

Fig. 4. DEI peak image recorded by X-ray film and its magnified image of the selected region. The energy of X-ray was 8 keV and stream intensity was 60 mA. (a) 1, basilar membrane; 2, basilar membranous crest; 3, cochlear duct; 4, spiral lamina; 5, vestibular membrane; 6, limbus of Hansen cell; 7, static cilia of hairy cell; 8, modiolus; 9, spiral prominence; 10, tympanic scala; 11, vestibular scala; 12, spiral limbus. (b) Bold arrow refers to basilar membranous crest; thin arrow refers to static cilia of hairy cell; thick arrowhead refers to limbus of Hansen cell; and asterisk refers to spiral limbus.

The spatial resolution of micron of DEI system depends on the spatial resolution of the detector. The spatial resolution of FDI camera used in our experiments is 10.9 μm and the resolution of resultant image is about 40 μm by estimating. However, the resolution of the X-ray film reaches 0.3—0.8 μm, so that DEI images recorded by X-ray film have higher contrast and better spatial resolution than digital ones. At the same time, X-ray film provides only analog images, which is too complicated to be digitalized, and not suitable for CT imaging. Therefore, the spatial resolution of the digital detector must be improved in order to achieve DEI-CT of cellular level.

3.2 Serial DEI images

A series of DEI images were acquired with the

analyzer crystal tuned to the selected serial points on the rocking curve, which is shown in Fig.3. Some of the resultant images are given in Fig. 5, in which (a)—(f) show DEI images acquired when the analyzer crystal was tuned to the low angle side, (h)—(l) show DEI images of the high angle side, and (g) shows the peak image. All images in Fig. 5 were recorded by FDI camera. Comparing with the conventional absorption-based image of the cochlea shown in Fig.6, all DEI images have higher contrast, clearer details and more effective edge enhancing. This is mainly because that all DEI images have obtained X-ray refraction contrast. This demonstrates that DEI technique is an obviously better way to observe inner structures of the minute organs and micro-tissues comparing with the conventional absorption-based X-ray imaging techniques.

By observing images in Fig.5 carefully, one may find that the low and high angle two-dimensional DEI images present obvious three-dimensional visional effects. The further away the peak point, the more obvious the three-dimensional visional effect is. And the peak image has no three-dimensional visional effect. The main reason, as it is analyzed, is that DEI images of the low and high angle sides contain more X-ray refraction contrast and less absorption contrast.

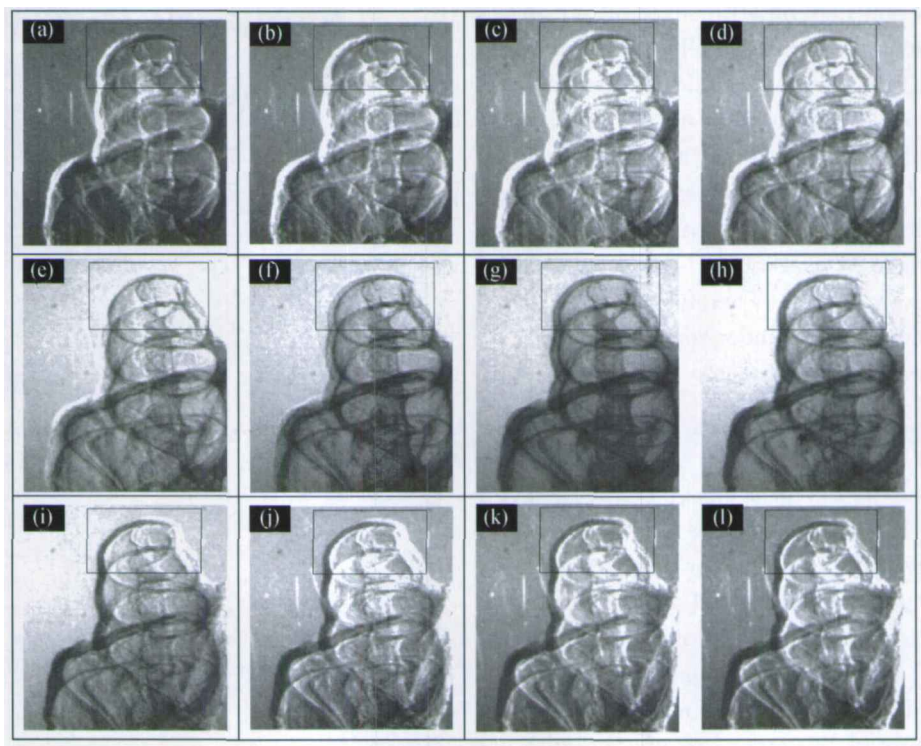

Fig. 5. The DEI images. (a)—(l) are acquired corresponding to the selected points on the analyzer rocking curve shown in Fig.3. The imaging parameters and analysis results of ROI are given in Table 2. The energy of X-ray was 9.4 keV and stream intensity was 54 mA.

DEI images acquired at the symmetric points on the rocking curve show opposite shadows of the certain structures. For example, in the images of Fig.5 (a)—(e) the left edges of the structures are very bright and the right edges are dark while the images of Fig.5 (i)—(l) show opposite edge shadow, e.g. the right edges are very bright and the left edges are dark. It is mainly due to the selective diffraction of the analyzer crystal to the refracted X-rays transmitting through the object. The contrast of DEI images acquired with the analyzer tuned to two shoulders of the rocking curve comes from the refraction index gradient distribution of X-rays inside the object. Due to the existence of X-ray refraction, the reverse phase shift gradient occurs at the left and right edges of the structures inside the object. At the same time, the different diffraction enhancing effects of the analyzer crystal at two shoulders of the rocking curve enhance the reverse phase shift gradient, which is expressed as reverse shadows of the left and right edges in DEI images. DEI images acquired close to the peak point on the rocking curve have no obvious reverse shadows.

Therefore, DEI images of the low and high angle sides show the obvious characteristic of the refraction-based image while DEI peak images show the characteristic of the absorption-based image. The DEI peak image derives contrast mainly from X-ray

absorption by the object and little from diffraction and scattering. Due to the scattering-rejection of the analyzer crystal, the DEI peak images are improved dramatically and contain higher contrast and better spatial resolution comparing with the conventional absorption-based image shown in Fig. 6.

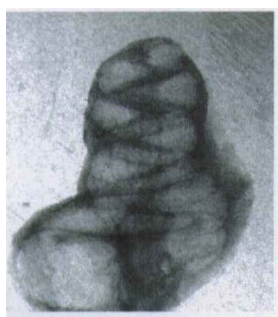

Fig. 6. The conventional absorption-based image of the cochlea. The energy of X-ray was 9.4 keV and stream intensity was 54 mA.

SNR and FOM were used to evaluate the quality of the DEI images and the imaging efficiency. We selected the regions at the same position in the serial DEI images as the regions of interest (ROI). The evaluation results of ROI for 24 DEI images acquired in the experiments are given in Table 2 and Fig. 7. Because of the reverse shadows of the left and right edges in DEI images, the pixel values of the valid signals in ROI are reverse. So it is impossible to compute directly the values of the signal using the pixel values. Our solution is computing the gradient distribution images of ROI using the Sobel operator. In these gradient distribution images, the pixels whose value is bigger than 40 (i.e. the gradient value is bigger than 40) are selected and their average value is referred to as the value of the signal. The standard deviation of the background pixels is referred to as the value of the noise. Then, SNR is computed out using signal to noise ratio. The bigger the SNR is, the clearer the image is, also the better the quality is; otherwise, the image quality is worse. When the radiation dose of the X-rays is taken into account, FOM values of DEI images are obtained based on SNR. FOM represents the performance-cost ratio of the image quality and the radiation dose. Its value is determined by both SNR and radiation dose. Table 2 gives SNR and FOM values of ROI in DEI images of Fig. 5. SNR curve and FOM curve of the 24 DEI images are shown in Fig. 7.

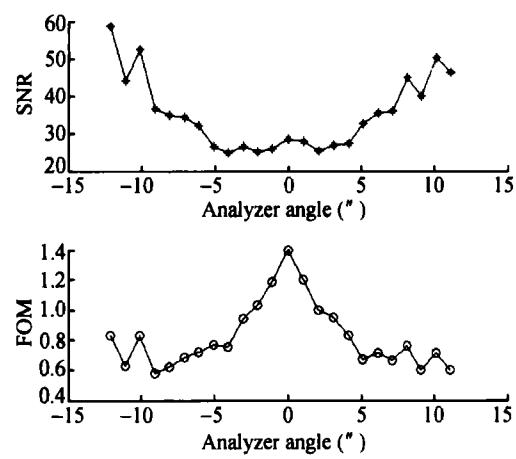

Fig. 7. SNR curve and FOM curve of the serial DEI images. The points on both curves correspond to the selected points on the rocking curve shown in Fig. 3.

Table 2. SNR and FOM values of ROI in the DEI images shown in Fig. 4

Image order	$\Delta I/I_0$	Exposure Time (ms)	SNR of ROI			FOM($\sqrt{\text{ms}}^{-1}$)
			Signal	Noise	SNR	
a	0.19	5000	57.85	0.9832	58.84	0.83
b	0.22	4000	65.45	1.2461	52.52	0.83
c	0.28	3200	67.85	1.9406	34.96	0.62
d	0.42	2000	68.89	2.1433	32.14	0.72
e	0.65	1100	68.14	2.7389	24.88	0.75
f	0.87	600	60.33	2.3840	25.30	1.03
g	0.99	420	55.41	1.9344	28.65	1.40
h	0.85	650	62.75	2.4651	25.46	1.00
i	0.63	1100	67.25	2.4451	27.51	0.83
j	0.41	2500	66.85	1.8851	35.46	0.71
k	0.27	3500	67.66	1.5057	44.94	0.76
l	0.21	5000	67.44	1.3422	50.25	0.71

Annotation: denote I_M(keV) as the energy of the monochromatic X-ray beam, T (ms) as exposure time, then the relative radiation dose is defined as $D_S = I_M \cdot T$ (unit is eV·s), and the equation of FOM is FOM = SNR/ $\sqrt{D_s}$. Comparing the relative radiation dose is equal to the comparing exposure time because that all DEI images were acquired in the same I_M. So, the equation of FOM becomes FOM = SNR/$\sqrt{T}$ in the Table.

SNR and FOM curves present contrary movement rules (Fig. 7): (1) on the U-shaped SNR curve, SNR value corresponding to the peak point of the rocking curve is smallest, which is located at the bottom of the curve, and is getting bigger when away from the peak point till reaching the biggest; (2) FOM curve looks like an upside down "V", e.g. FOM value is biggest corresponding to the peak point, getting smaller fast away from the peak point. So DEI method provides smaller SNR and the biggest FOM at the peak point of the rocking curve, and provides smaller SNR and FOM close to the points of $\mp\theta_D/2$. This comes from the big differences of the exposure time aroused by the big differences of diffraction efficiency to the transmitted X-rays by the analyzer crystal. As to DEI shoulder images, bigger SNR costs more radiation dose.

Moreover, both the SNR and FOM curves are symmetric incompletely. The incomplete symmetry is due to two reasons. One of them is that the light aperture floating results in incomplete symmetry of the symmetric points on two shoulders of the rocking curve when the analyzer crystal is rotating. The other is the influence of errors in computing SNR and FOM.

3.3 The apparent absorption and refraction images

Primary characteristic of DEI is that it can separate the refraction information from others and provide the apparent absorption and refraction images. Since it is difficult to accurately set completely symmetric points on the rocking curve in the experiments, as it was discussed above, we select Eqs. (2a) and (2b) to compute the apparent absorption and refraction images. Fig. 8 gives the obtained apparent absorption and refraction images.

The apparent absorption image mainly derives contrast from X-ray absorption while the apparent refraction image derives contrast from phase shift by X-ray refraction. In DEI method, the analyzer crystal has natural ability of scattering-rejection. So DEI is a scattering-free imaging method. The apparent absorption and refraction images were computed out on the precondition that the influence of X-ray small-angle scattering could be ignored.

In the apparent absorption image shown in Fig. 8 (a), the bright capula of cochlea with smaller thickness explains characteristic of low absorption, while the dark base of cochlea with unidentifiable structures explains high absorption.

Contrarily, the apparent refraction image shown in Fig. 8 (b) intensively presents the characteristic of phase-contrast image with obvious effect of edge enhancing and oriented phase gradient, for example, the left inner wall of the cochlea has darkly edge-enhanced effect and the right inner wall shows very bright edge-enhanced effect. Moreover, the apparent refraction image shows stronger three-dimensional visional effect over the low and high angle images in Fig. 5. However, its contrast and spatial resolution decrease a little due to errors in data processing.

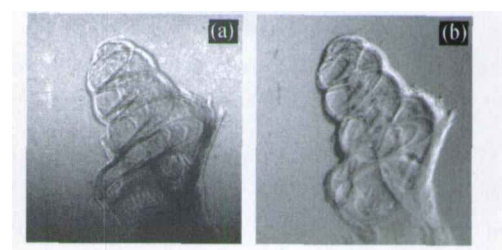

Fig. 8. The apparent absorption and refraction images of the guinea pig cochlea. (a) The apparent absorption image; (b) the apparent refraction image.

The apparent refraction image mainly contains refraction contrast of X-rays. It provides a bigger FOM with a little decrease of SNR. The advantages of the high contrast but low radiation dose will boost its clinical applications.

4 Conclusions

With DEI method to image the cochleae, the acquired images display clearly not only the holistic spiral structure of the cochleae and inner details, but also those structures at cellular level, such as static cilia of hair cells, limus of Hensen cell, and so on. As experimental results demonstrate, DEI dramatically improves the contrast and spatial resolution of images. So DEI is a promising tool for biological and medical researches. Another characteristic of DEI is the obvious effect of edge enhancing. This inherent edge-enhanced effect of DEI has potential uses in edge detecting, object recognizing and clinical diagnosis.

From SNR and FOM analyses to the serial DEI images derived at a serial of points on the analyzer rocking curve, it is found that DEI images corresponding to different points on the rocking curve have different qualities, for example, DEI image from the low shoulder of the rocking curve has bigger SNR but

smaller FOM. Therefore, it is necessary to synthetically evaluate the images with image quality and imaging efficiency when DEI is used in imaging the biological tissues. The clinical applications of the radiography demand high image quality as well as low radiation dose exposed to the patient. The apparent refraction image has the potential to satisfy these two demands. The contrast of the apparent refraction image mainly comes from the refraction gradient distribution of X-rays inside the object. It decreases the radiation dose while assuring the high resolution of the image.

Since the spatial resolution of DEI depends on the detector, the spatial resolution of the digital detector must be improved in order to acquire DEI images with higher resolution. Also, DEI projected images superimposed three-dimensional object's information onto two-dimensional images. So it is difficult to determine the exact spatial locations of the interested structures in the two-dimensional DEI images. We expect to achieve DEI-CT at cellular level with the development of the digital detector and CT reconstruction algorism.

To sum up, as a brand-new imaging method, DEI has its inherent advantages and characteristic. More theoretical researches and more experiments on biological tissues are needed to boost its applications in biology, medicine and clinic.

Acknowledgement The authors thank Prof. Zhu Peiping, Dr. Shu Hang, Dr. Yuan Qingxi, Dr. Huang Wanxia, Dr. Wang Junyue and Zheng Xin from Beijing Synchrotron Radiation Facilities (BSRF) for assistance in our experiments; thank Wang Chen, Shi Xin, Chen Jing, Chen Xiang, Feng Jian, Zhang Junyi and Lu Xiang from Medical Image Laboratory of Capital University of Medical Sciences for assistance and helpful advices.

References

1 Gao D. C., Pogany A., Stevenson A. W. et al. Hard X-ray phase contrast imaging. Acta Physica Sinica (in Chinese), 2000, 49(12): 2357—2368.
2 Tian Y. L., Xiao T. Q., Zhu P. P. et al. Synchrotron X-ray phase contrast imaging—X-ray phase contrast radiography. Nuclear Techniques (in Chinese), 2004, 27(6): 417—421.
3 Momose A. and Fukuda J. Phase-contrast radiographs of nonstained rat cerebellar specimen. Med. Phys., 1995, 22: 375—380.
4 Momose A., Takeda T. and Hirano K. Phase-contrast X-ray computed tomography for observing biological soft tissues. Nature Medicine, 1996, 2: 473—475.
5 Davis T. J. and Gao D. Phase-contrast imaging of weakly absorbing materials using hard X-rays. Nature, 1995, 373: 595—597.
6 Fitzgerald R. Phase-sensitive X-ray imaging. Physics Today, 2000, 53(7): 23—26.
7 Momose A. Demonstration of phase-contrast X-ray computed tomography using an X-ray interferometer. Nuc. Instrum. Meth. Phys. Res., 1995, 352: 622—628.
8 Momose A. Phase-sensitive imaging and phase tomography using X-ray interferometers. Optics Express, 2003, 11: 2303—2314.
9 Chapman D., Thomlinson W., Johnston R. E. et al. Diffraction enhanced X-ray imaging. Phys. Med. Biol., 1997, 42: 2015—2025.
10 Dilmanian F. A., Zhong Z., Ren B. et al. Computed tomography of X-ray index of refraction using the diffraction enhanced imaging method. Phys. Med. Biol., 2000, 45: 933—946.
11 Li G., Wang N. and Wu Z. Y. Hard X-ray diffraction enhanced imaging only using two crystals. Chinese Science Bulletin, 2004, 49(19): 1930—1936.
12 Koyama I., Hamaishi Y., Momose A. et al. Phase tomography using diffraction-enhanced imaging. AIP Conference Proceedings, 2004, 705: 1283—1286.
13 Oltulu O., Zhong Z., Hasnah M. et al. Extraction of extinction, refraction and absorption properties in diffraction enhanced imaging. J. Phys. D: Appl. Phys., 2003, 36: 2152—2156.
14 Oltulu O. A unified approach to X-ray absorption-refraction-extinction contrast with diffraction enhanced imaging. Ph. D. Thesis (UMI Number: 3087854), Illinois Institute of Technology, USA, 2003.
15 Wilkins S. W. and Gureyev T. E. Phase-contrast imaging using polychromatic hard X-rays. Nature, 1996, 384: 335—338.
16 Stevenson A. W., Gureyev T. E., Paganin D. et al. Phase-contrast X-ray imaging with synchrotron radiation for materials science applications. Nuc. Instrum. Meth. Phys. Res. B, 2003, 199: 423—435.
17 Voie A. H. Imaging the intact guinea pig tympanic bulla by orthogonal-plane fluorescence optical sectioning microscopy. Hearing Research, 2003, 171: 119—128.
18 Sugawara M., Ishida Y. and Wada H. Mechanical properties of sensory and supporting cells in the organ of Corti of the guinea pig cochlea-study by atomic force microscopy. Hearing Research, 2004, 192: 57—64.
19 Pagot E., Fiedler S., Cloetens P. et al. Quantitative comparison between two phase contrast techniques: diffraction enhanced imaging and phase propagation imaging. Phys. Med. Biol., 2005, 50 (4): 709—724.
20 Keyriläinen J., Fernández M., Fiedler S. et al. Visualisation of calcifications and thin collagen strands in human breast tumor specimens by the diffraction-enhanced imaging technique: a comparison with conventional mammography and histology. Eur. J. Radiol., 2005, 53: 226—237.